Analysis of laterally-coupled-cavity VCSELs for ultra-high-frequency photon-photon resonance modulation

Analysis of laterally-coupled-cavity VCSELs for ultra-high-frequency photon-photon resonance modulation

N. Ledentsov Jr.*[a], V. A. Shchukin[a], Ł. Chorchos[a], O. Yu. Makarov[a], J.–R. Kropp[a], I. E. Titkov[a], V. P. Kalosha[a], V. Zerova[a], M. Lindemann[b], N. C. Gerhardt[b], M. D'Alessandro[c,d], V. Torrelli[c,d], P. Debernardi[d], A. Tibaldi[c,d], M. R. Hofmann[b] and N. N. Ledentsov[a]

[a] VI Systems GmbH, Berlin, Germany
[b] Photonics and Terahertz Technology, Ruhr-Universität Bochum, Bochum, Germany
[c] Department of Electronics and Telecommunications, Politecnico di Torino, Turin, Italy
[d] Consiglio Nazionale delle Ricerche, IEIIT Torino and VCSELence Torino, Turin, Italy

ABSTRACT

We report high frequency (20-100 GHz range) optical field intensity oscillations in laterally-coupled-cavity vertical-cavity surface-emitting lasers with several different techniques. The oscillation frequency is defined by the photon energy splitting of the coupled states. The resonance effect is stable in an extended current range and can enable modulation frequency resonances at higher frequencies as compared to the conventional relaxation oscillation frequency of the laser. This paves a way towards high-speed data transmission solutions at data rates beyond ~200 Gb/s with the advantage of better laser stability, as the resonance observed can reach high frequencies even at low current densities.

A ~75 GHz intensity modulation between optical modes of a coupled-cavity VCSEL array was first reported by the authors in a two-aperture configuration in 2023 applying optical excitation [1]. Studies of 4- and 10-element coupled VCSEL arrays give further insight into the effects observed. New 3D numerical simulations and electrical modulation techniques have been applied to address the specific nature of the photon-photon resonance studies.

Keywords: vertical cavity surface–emitting laser, data transmission, high-frequency, resonance

1. EXTENSION OF VCSEL MODULATION BANDWIDTH VIA PHOTON-PHOTON RESONANCE

High frequency performance of a VCSEL is governed by the intrinsic laser response as well as by the extrinsic parasitic response [2]. Particularly, VCSELs operating at datacom wavelengths ranging from 830 nm to 1100 nm are based on GaAs/GaAlAs structures. The modulation bandwidth (i. e., (–3dB) cutoff frequency) is governed by the differential gain, which can be maximized by applying the antiwaveguiding concept [3] which maximizes the optical confinement factor of the VCSEL mode in the active medium and employing compressively strained GaInAs multiple quantum wells as the active medium. Typically (–3dB) cutoff frequency for GaAs–based VCSELs is about 30 GHz [4], which can hardly be significantly increased just by fine tuning of the chip design.

A pathway to achieve a significant increase of the modulation bandwidth is to employ the photon–photon resonance. Once an optical system contains two or more optically coupled elements, and thus supports at least two optical modes with a small spectral separation, beats at a frequency equal to the difference of the two modes become possible. E.g., for a device operating at 850 nm, the spectral separation of, 0.2 nm implies a difference frequency $\boldsymbol{f_{\text{diff}} = c(\Delta\lambda)/\lambda^2 \approx 83}$ GHz, where *c* is the velocity of light**.** Such beats influence the modulation transfer function at this range of frequencies and may result, additionally to the carrier–photon resonance at the relaxation oscillation frequency, also in a second, photon–photon resonance at a higher frequency. However, a real improvement of the high–frequency performance of the VCSEL remains challenging since one needs to provide a rather flat modulation transfer function from 0 to a high cutoff frequency. Thus, such effect was explored for edge–emitting distributed Bragg reflector lasers [5, 6, 7] with detuned Bragg reflector, wherein the interaction between a high Q–factor mode of the active section and a low Q–factor mode of the passive section allows

* Corresponding author: Nikolay Ledentsov Jr., Tel.: +49 30 308314347; E–mail: nikolay.ledentsov-jr@v-i-systems.com

Vertical-Cavity Surface-Emitting Lasers XXVIII, edited by Chun Lei, Kent D. Choquette, Proc. of SPIE
Vol. 12904, 1290405 · © 2024 SPIE · 0277-786X · doi: 10.1117/12.3001177

extension of the bandwidth up to 70 GHz. By applying this concept, a modulation bandwidth of 108 GHz was demonstrated, and the data transmission with an open eye diagram at 256 Gb/s was realized [8].

An approach similar to some extent is based on a master–slave coupled laser system, wherein the optical injection of the laser light emitted by a master laser can force a slave laser to lase at the wavelength of the master light [9]. Such regime of the optical injection locking realized under certain values of the frequency detuning and injection ratio affects the modulation response curve of the slave laser and may result in a significant enhancement of the modulation bandwidth of it. Thus, the modulation bandwidth of 80 GHz was demonstrated for a master–slave system of VCSELs [10]. Yet another approach employs feedback cavities. Thus, laser light emitted by a VCSEL can be optically coupled in the lateral plane with one or several passive cavities. The laser light leaks from the active device, travels in the lateral direction through the passive cavity, is back–reflected, returns to the active cavity with some time delay thus realizing beating with the primary light at a zero frequency detuning [11]. VCSEL with a hexagonal array of 6 passive cavities demonstrates the modulation bandwidth of 45 GHz [12], and theoretical predictions for such a system suggest a possible bandwidth of 160 GHz under properly optimized parameters [13].

One of key parameters affecting the photon–photon resonance is an overlap integral between two modes. It was emphasized in [7], with a focus on DBR edge–emitting lasers, that the cavity of a laser is always open and dissipative, and that different longitudinal modes are not completely power orthogonal, and can be coupled with each other. The coupling between the master and slave optical modes in a master–slave laser system determines the optical injection ratio and, thus, affects the parameter range of the stable injection locking. For VCSELs, a nearly 100% overlap integral between the spatial profiles of the two fundamental transverse optical modes with two orthogonal polarizations is promising once there is a non–zero optical coupling between these modes. Such coupling is known to exist due to spin relaxation [14, 15, 16]. Further mechanisms contributing to the coupling are birefringence and gain anisotropy [17, 18]. By mechanically applied strain to a VCSEL, the birefringence splitting of the two optical modes >250 GHz was observed [19] indicating a high potential for increasing the VCSEL modulation bandwidth.

Those effects, namely a combination of spin relaxation, birefringence and gain anisotropy, render also possible the optical coupling of an optical mode of a VCSEL with an orthogonally polarized injection light. Thus, experimental studies of orthogonal optical injection in a master–slave laser system with a VCSEL as a slave laser [20] have demonstrated a broad parameter region of optical injection locking. These observations suggest a mechanism for the observed orthogonal polarization of the emitted laser light from two coupled VCSELs of a VCSEL mini–array.

2. MANUFACTURED VCSEL STRUCTURES

To study the resonances in coupled cavities, we have manufactured linear VCSEL arrays in which neighboring apertures are put at <10μm distance between each other to enable coupled emission and energy transfer. Figure 1 shows microscope images of manufactured VCSELs arrays with two, four and ten elements. Figure 2 shows infra-red images in which the oxide aperture size is visible as well. Due to different microscope settings that were needed to capture the 10-element array, the apertures there are not well visible but are similar to other arrays. The aperture size was selected to have single-mode or quasi-single-mode emission from each of the array elements.

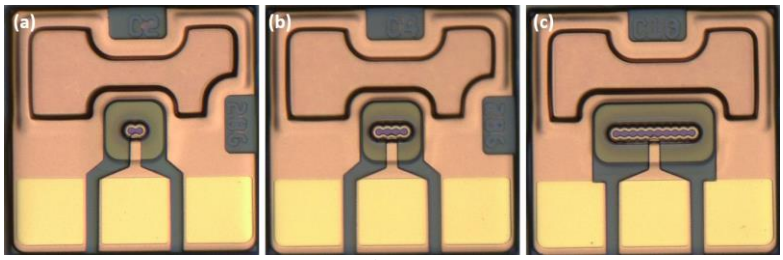

Figure 1: Images of linearly coupled VCSEL-arrays with (a) two and (b) four and (c) ten elements.

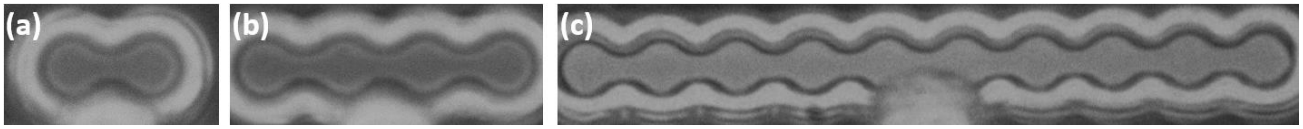

Figure 2: Infra-red images representing oxide apertures of linearly coupled VCSEL-arrays with (a) two, (b) four elements and (c) ten elements (here the aperture size is less visible due to a different microscope configuration)

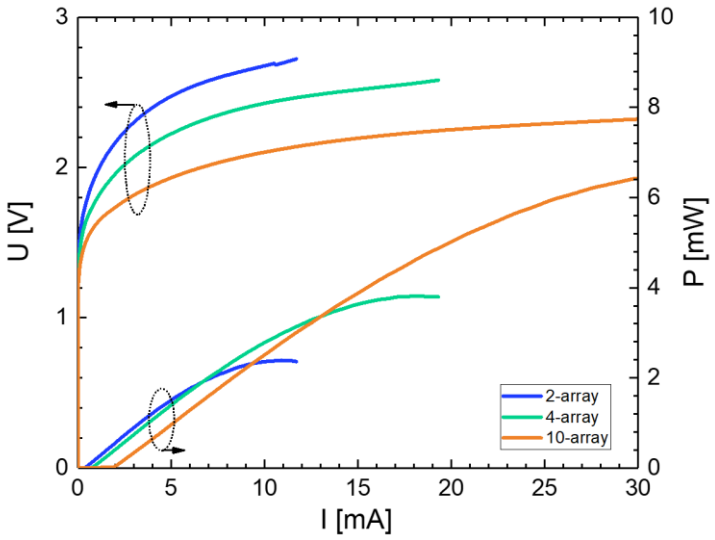

Figure 3: Light, Voltage, Current characteristics of the arrays studied.

3. MEASUREMENT TECHNIQUES

To measure the resonance, several methods are employed. A) If the laser is modulated with a sinusoidal signal of a specific frequency, the intensity of the optical modulation can be measured with an oscilloscope. B) Small-signal modulation measurements performed with Vector Network Analyzers (VNA) reveal the same resonance peaks. C) Relative Intensity Noise (RIN) measurements performed with Electrical Spectrum Analyzer (ESA) reveal resonance peaks, as noise is amplified at these frequencies and D) Measurement of oscillations with a streak camera after pulsed optical injection.

As the last method is not typical for the characterization of VCSELs, we describe it in a little more detail in Figure 4. The VCSEL array is excited with a Ti:sapphire (Ti:Sa) 810 nm laser 200 fs pulses with 75.6 MHz repetition rate, with an average power of 1 mW, linearly polarized in the axis of the array elements. A more detailed description of this method can be found in Refs. [1, 21]

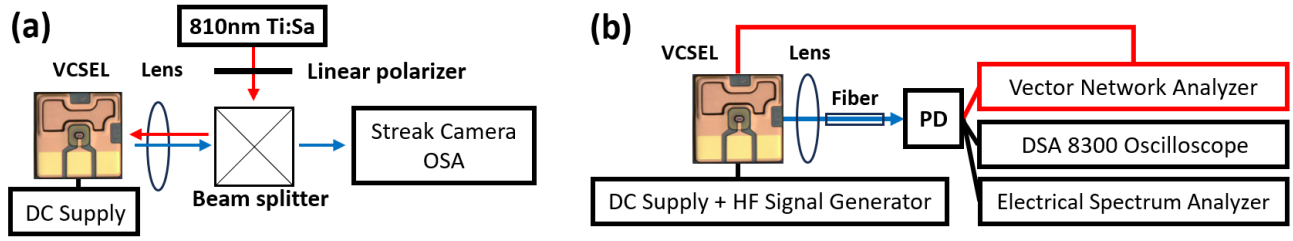

Figure 4: (a) A hybrid pumping scheme which combines a continuous electrical bias current with optical pumping pulses through Ti:Sa laser and (b) traditional setup for characterization of VCSEL emission in high-frequency domain, with VNA, DSA and ESA.

The output light of the VCSEL array is directed through the beam splitter towards a Hamamatsu S-1 cathode streak camera or to a Yokogawa AQ6370DHR optical spectrum analyzer (OSA). The streak camera is operated with an 800 ps time window and features a temporal resolution of 9.3 ps. Beams originating from different elements of the array can be analyzed separately in the streak camera.

A combination of all these measurement techniques is used in this paper. Peaks visible in RIN or in VNA-measured frequency response can be of different nature, but the analysis performed with the streak camera enables a detailed glimpse into the processes with extremely high spatial and temporal resolution. While a streak camera enables the study of resonances up to 200 GHz, other methods only allow the study of effects occurring below 40 GHz due to equipment limitation. Moreover, because the photodiode used in traditional setup has ~35 to 40 GHz bandwidth, effects occurring at very high frequencies have usually very small amplitude and are strongly affected by the noise of the equipment.

3. STUDY OF RESONANCES WITH 2-APERTURE LINEAR VCSEL ARRAYS

The analysis of the resonance occurring was already presented in Ref. 1, but here we add some new details and present the results that enable comparison of the particular features of the arrays studied to other array structures.

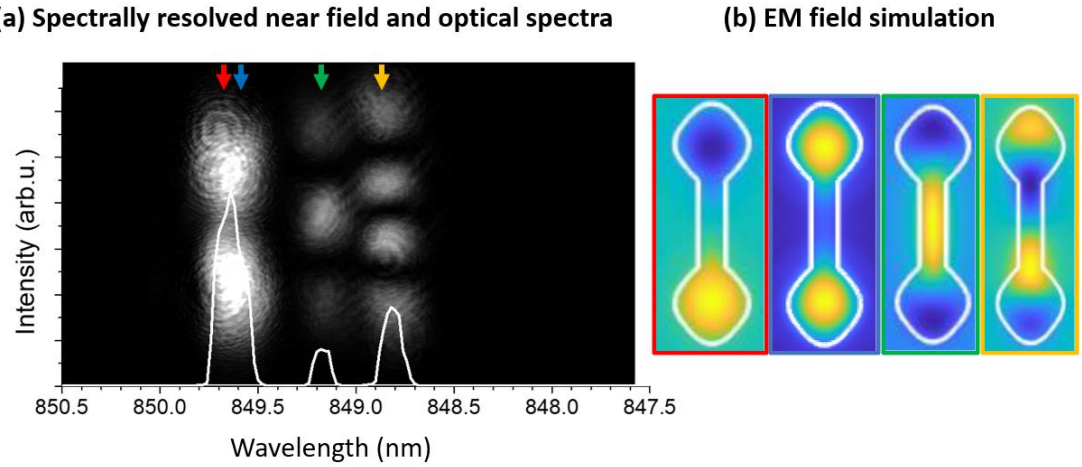

Figure 5: (a) Spectral measurement and spectrally resolved near-field of a two-element array at ~3mA and (b) electromagnetic simulations of the supermodes emitted from the structure.

Figure 5(a) shows spectra and spectrally-resolved near-field of a two-element array overlayed over each other, enabling quick identification of the spectral modes. The simulation of the device is performed by means of our in-house VCSEL Electro Magnetic 3D vectorial suite VELM [22, 23] which, starting from the description of the 3-dimensional (3D) refractive index profile, can calculate the VCSEL modes together with their emission frequencies, their longitudinal confinement factors, and their threshold gains. Figure 5(b) shows numerical simulations of the electromagnetic field of the supermodes supported by a 2-element array. Those are identical to the measured near-field profiles in Fig. 5(a). Simulation predicts a mode splitting and resonance of 20 GHz between the first odd (red) and even (blue) supermodes in an ideal case of equal apertures without temperature effects.

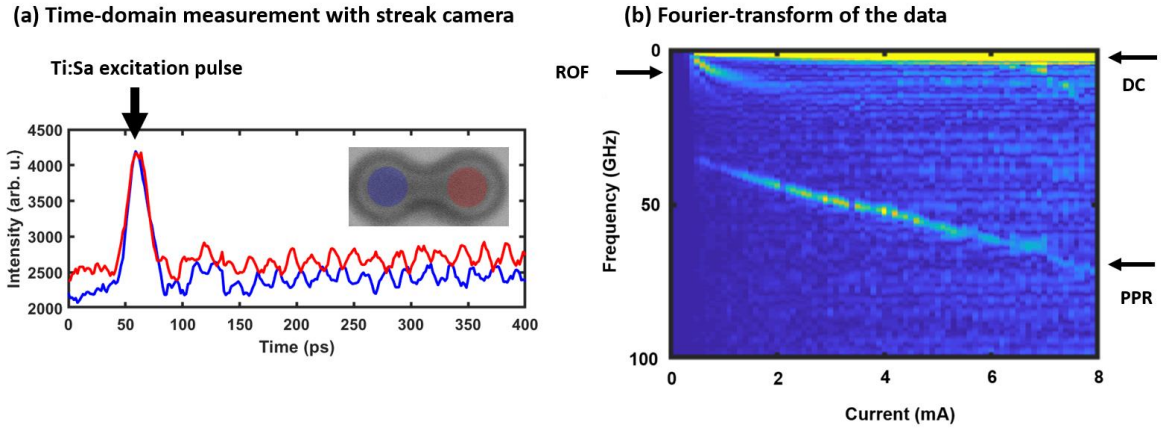

Figure 6: (a) Intensities of the two cavities under pulsed pumping at 4 mA bias current. The red (blue) trace corresponds to the left (right) aperture. (b) Fourier-transform of the acquired data at different currents represented in a heat map.

This sample is then measured using the techniques described above and with the external pulse excitation. As mentioned before, small-signal modulation or oscilloscope studies are limited by the frequency response of the receiver, this is why they can be used only for studies of resonances <40 GHz. To study resonances >40 GHz a streak camera has to be used. Despite some variations depending on the chip studied, both experimental methods show similar effects that can be well-matched to numerical simulations and give insight into the physics behind these processes.

Once the VCSEL is illuminated with the external optical pulse, one can observe relaxation oscillations, containing both a typical resonance frequency and photon-photon-resonance effects. Figure 6(a) shows the raw acquired data of the relaxation oscillations separated into the two elements of the array. The first peak observed after the pumping pulse at approximately t = 60 ps, followed by a strongly damped and slow oscillation with a second peak visible at around 120 ps. This corresponds to the intensity relaxation oscillation frequency (ROF) of ~10 GHz. After the first strongly damped peak, a faster and more persistent (weakly damped) oscillation of ~50 GHz is observed in both array elements. The peaks of the oscillation in both array elements are in antiphase, which clearly shows that this is an effect occurring inside the VCSEL and is not a function of the receiver.

Figure 6(b) shows Fourier transform data of the acquired signals at various bias currents from 0 to 8 mA for one of the apertures. This plot clearly shows the resonance frequency (ROF) of the laser that is strongly damped through heating occurring due to bias current. A stable sharp peak linearly increasing with the current can be attributed to the photon-photon-resonance (PPR) between the first odd and even supermodes. This analysis enables a correct interpretation of the PPR peaks observed in the S21 frequency response measurements acquired from two-aperture arrays displayed in Fig 7(b). Selected Fourier-transformed spectra displayed in Fig 7(a) show very similar positions of the resonance peaks under external optical excitation as the electrical frequency response data, although both spectra were acquired on slightly different samples.

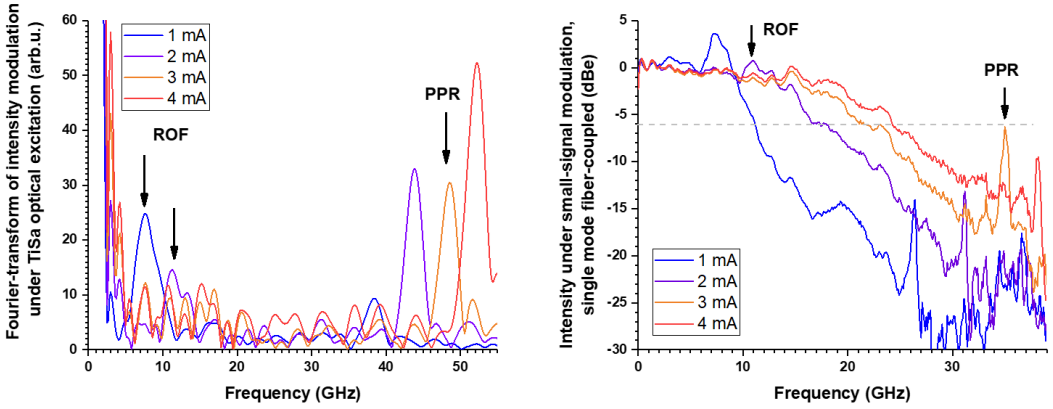

Figure 7: (a) Fourier-transform of the data acquired with the streak camera at different bias currents. (b) Normalized S21 VCSEL frequency response spectra measured with single-mode fiber coupling with VNA at the same currents, showing similar position of the ROF and PPR peaks.

Because the oscillation between the apertures is occurring in anti-phase, the best observation of the effect can be done with coupling to only one of the two apertures, for example, through coupling into single mode fiber (SMF). This is why Figure 7(a) and Figure 8 are acquired with single-mode fiber coupling to differentiate between the left and right aperture.

Figure 8 shows the spectra and the frequency response acquired under such conditions in detail at different currents for a VCSEL with a particularly strong resonance peak. A possible reason why this sample is different from a sample discussed previously (that was measured both with small-signal modulation and in optical excitation with streak camera), is that in this sample the resonance occurs at lower frequencies and has therefore a higher intensity of the signal. Figure 8(a) shows the optical spectra acquired under the single-mode fiber-coupling, clearly showing the intensity difference between the mode originating in the right and the left apertures, depending on the coupling. Figure 8(b-c) shows a small signal response acquired on this chip under these conditions.

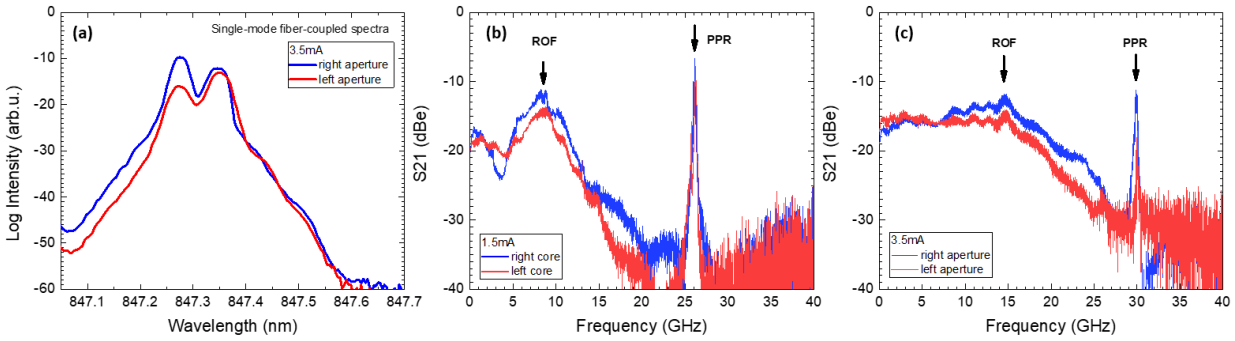

Figure 8: (a) Optical spectra of the first mode group acquired with single-mode fiber coupling at 3.5 mA, (b-c) Small-signal frequency response measured on a VCSEL with a very strong resonance peak, compensated for the photo-diode response.

The presence of the resonance is also observed in the sampling oscilloscope (Figure 9). Due to the coupling losses to the single-mode fiber, the acquisition of the signal is complicated. Still, by pre-selecting a VCSEL which has PPR resonance frequency <40 GHz (equipment limit) at high currents, one can detect a strong enough signal that is higher than the equipment noise and observe the resonance.

In this experiment the VCSEL is driven by a high-frequency signal generated by the SHF Synthesized Clock Generator that enables a supply of a modulation of a specific frequency to the VCSEL. Figure 9 and Figure 10 show the behavior of the resonance measured with the oscilloscope at bias currents of 1mA and 3mA. If driven at very low current (1mA), the ROF is located at ~7 GHz and the PPR is located at ~22.5 GHz (Figure 8(b)). Due to very low bandwidth at this current, at modulation above 20 GHz the signal is completely lost at the noise level (Figure 9(a)). But once the modulation frequency hits the resonance (Figure 10(c)), a clear modulation can be observed.

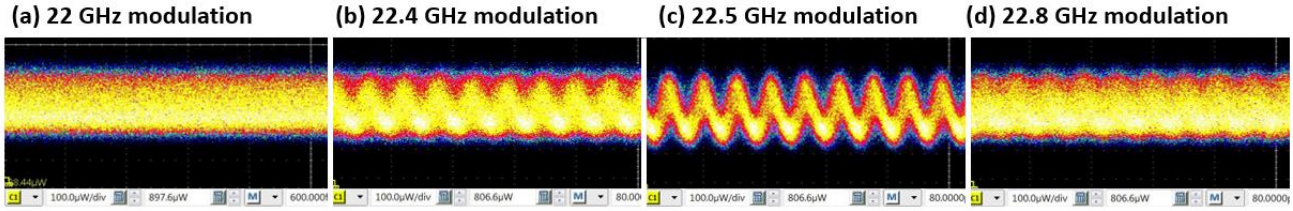

Figure 9: Signal measurements with oscilloscope under same bias and oscilloscope measurement conditions (vertical scale 100 µW/div) at 1 mA bias. Under (a) 22 GHz, (b) 22.4 GHz, (c) 22.5 GHz and (d) 22.8 GHz small-signal-modulation.

The same behavior can be observed at 3 mA, with the difference, that the resonance is located at higher frequency of ~38 GHz (Figure 10(c)), and due to higher signal intensity and higher intrinsic bandwidth of the VCSEL, the modulation intensity is slightly visible before the resonance (Figure 10(b)). Above the resonance frequency, the signal returns once more into the noise and is barely visible (Figure 10(d)).

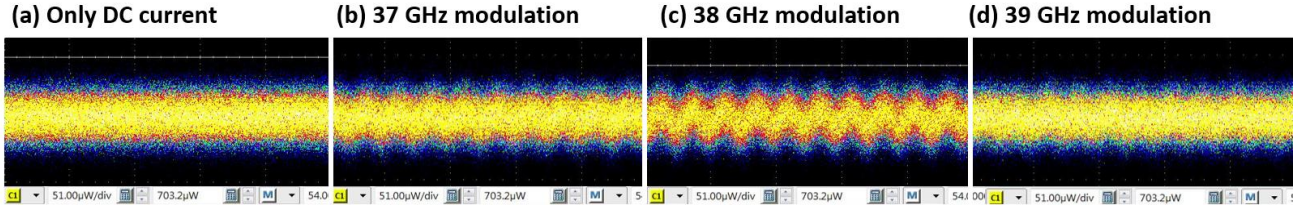

Figure 10: Signal measurements with oscilloscope under same bias and oscilloscope measurement conditions (vertical scale 51 µW/div) at 3.5 mA bias. Under (a) DC current, (b) 37 GHz, (c) 38 GHz and (d) 38 GHz small-signal-modulation.

As can be seen from these measurements, the limitation of the resonance in such a structure is that the resonance is observed at very high frequencies, where the modulation amplitude is very low. In order to use it constructively for the extension of the VCSEL bandwidth, one would prefer a wider resonance. Slight differences in the noise amplitude and the location of the resonance among different measurements occur because many measurements were taken on different VCSELs under slightly different coupling conditions.

4. STUDY OF RESONANCES WITH N-APERTURE LINEAR VCSEL ARRAYS

According to simulation, it is expected that arrays with more than two elements should have optical modes that are spectrally located closer to each other and thus the resonance between them should occur at lower frequencies. To confirm this hypothesis, we study the VCSEL arrays with 4 and 10 elements.

Figure 11(a) shows measured spectrally resolved near-fields of a 4-element array at different currents. Similar to the 2-element array, they correspond well with the EM field simulations shown in Figure 11(b).

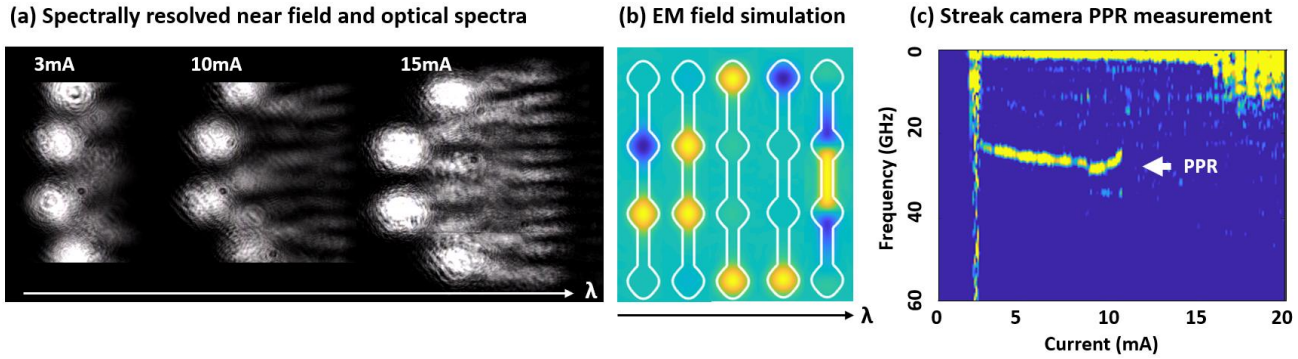

Figure 11: (a) Spectrally resolved near-field of a four-element array at different currents, (b) EM simulations of the supermodes emitted by the structure and (c) Externally excited streak camera data acquired at different currents, Fourier-transformed.

Streak camera measurements represented in Figure 11(c) confirm the hypothesis that the resonance frequency will be reduced by the 4-array element symmetry and show a resonance occurring between the first two supermodes at ~25 GHz. This is a reduction of the resonance frequency by a factor from 2 to 3 compared to a 2-element array (Figure 6). Due to larger dimensions of the array and thus much higher coupling losses compared to 2-element array, a fiber-coupled measurement was not yet performed for this chip. The same issue occurred in the study of 10-element array (Figure 12).

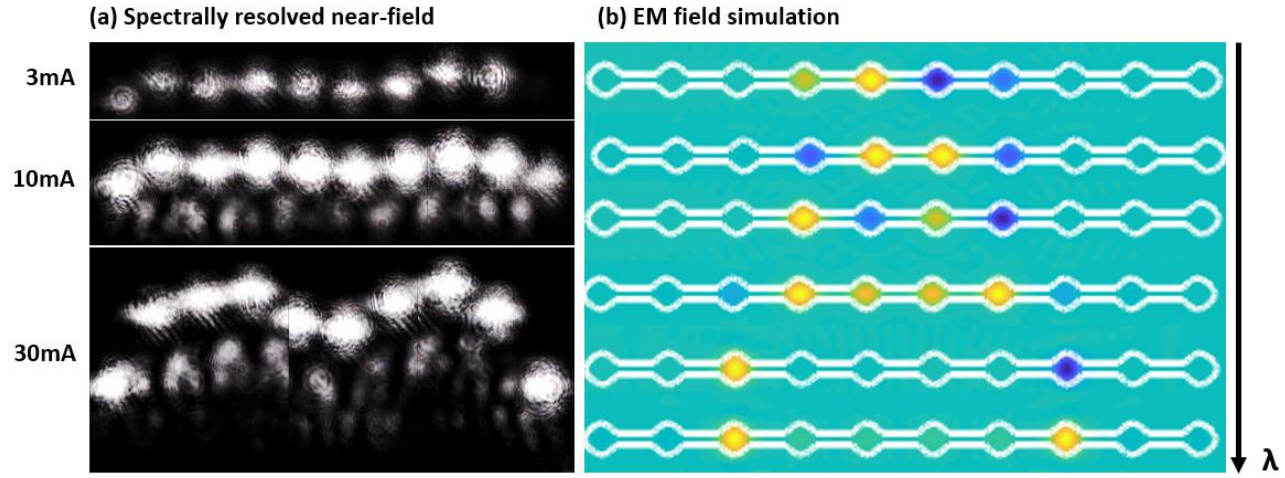

Figure 12: (a) Spectrally resolved near-field of a ten-element array at different currents and (b) EM simulations of the supermodes emitted from the structure.

Moreover, based on the near-field measurements (Figure 12(a)) it seems that a 10-element-array is much more sensitive to the inhomogeneous overheating of the array and thus the mode structure cannot be accurately predicted by EM simulations (Figure 12(b)) which does not include those effects. Regardless of this, the mode distance between the supermodes is, as expected, further reduced compared to two- and four-element arrays.

5. PATHS TOWARDS INCREASED CONTROL OVER THE RESONANCE BEHAVIOUR

In conclusion we show a series of simulations that confirm the interpretation of the effects presented in this paper and show how the resonance frequency, amplitude and width can be influenced. The simulations were performed on the basis on the inhomogeneous scalar wave equation [24] and are described in detail in Ref. 25. One of the factors that can influence the resonance to enable its fine-tuning is the gain difference of the supermodes. Figure 13 shows a simulation of a frequency response of a two-aperture array structure with a simulated gain difference between the first odd and even supermodes. The resonance width can be engineered by the modal gain difference.

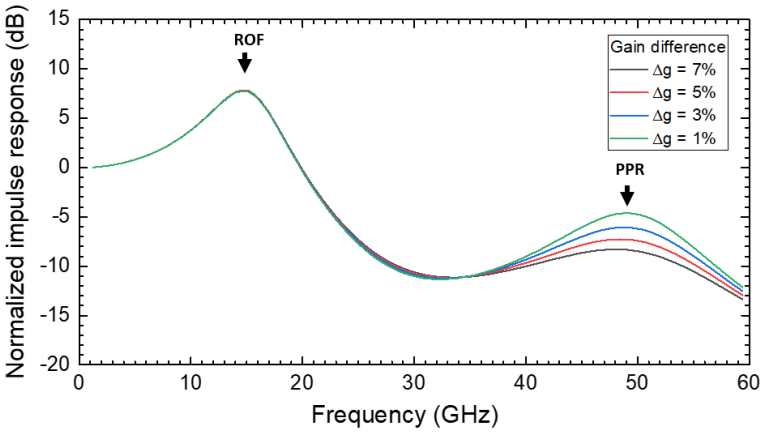

Figure 13: Numerical simulations of a frequency response of a two-aperture array structure with a simulated gain difference between the first odd and even supermodes.

The gain difference between the modes can be achieved through surface gratings, coatings or patterning of one of the apertures, for example, through etching, as shown in the images below (Figure 14). Selected etching of the part of the dielectric cap and of the several top DBR periods allows manipulation in external losses in one of the cavities paving the way towards controllable broadening of the PP resonances. The work in these directions is ongoing.

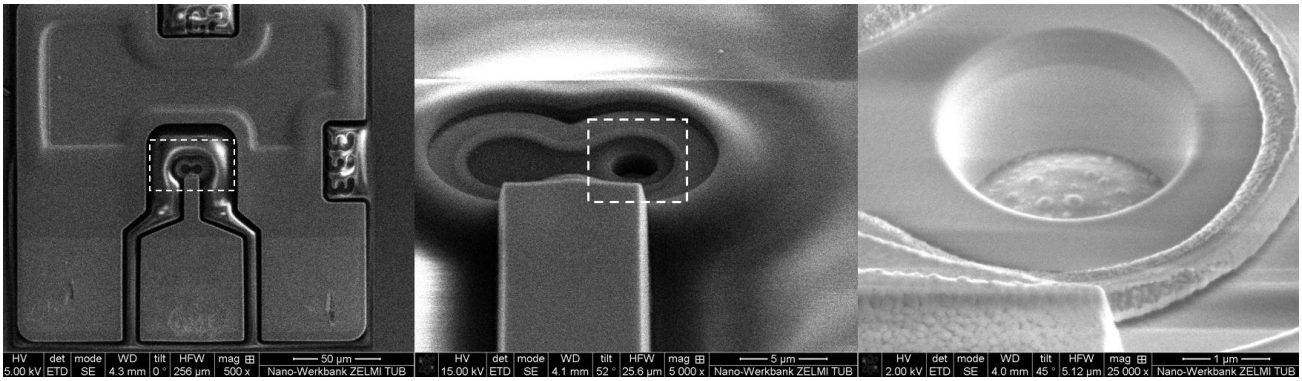

Figure 14: Electron microscopy images of Selected etch of the part of the dielectric cap and of the several top DBR periods applied to intestinally detune external losses in one of the cavities.

CONCLUSION

Coherently coupled VCSEL array are progressing towards industrial applications. A strong coupling between the resonating modes is preferable to ensure strong PP resonance features, while gain/loss mismatch between the interacting cavities is important to broaden the frequency resonances. High reflection, anti-reflection or absorbing coatings allow selective outcoupling of light of the interacting modes enhancing the frequency resonance. The work is critical for the next generation of VCSELs for data communications at -3 dB modulation bandwidths of ~40-100 GHz and beyond and for applications in optical computing based on coherently-coupled photon states. Long chains of coupled apertures are important for beam steering in sensing applications and in reconfigurable optical wireless networks. Novel designs based on coherent coupling and switching in VCSEL arrays pave the way towards applications in quantum computing and artificial intelligence.

ACKNOWLEDGMENT

Work on coupled VCSEL arrays was funded by the German Federal Government Programme for Research and Innovation (BMBF) 2021-2024 (Green-ICT) under the project Nr. 16ME0426K (E4C). We also acknowledge Dr. Christian Guenther from the Center for Electron Microscopy (ZELMI) of the Technical University of Berlin for the acquisition of the SEM images.

REFERENCES

[1] Lindemann, M., Gerhardt, N.C., Hofmann, M.R., Ledentsov, N., Shchukin, V.A., Ledentsov, N.N., Makarov, O.Y. and Turkiewicz, J.P., 2023, July. Coupled Aperture VCSELs Suitable for 100 GHz Intensity Modulation. In 2023 23rd International Conference on Transparent Optical Networks (ICTON) (pp. 1-4). IEEE.
[2] Chang, Yu-Chia, and Larry A. Coldren. "Design and performance of high-speed VCSELs." In VCSELs: Fundamentals, Technology and Applications of Vertical-Cavity Surface-Emitting Lasers, pp. 233-262. Berlin, Heidelberg: Springer Berlin Heidelberg, 2012.
[3] Ledentsov, N. N., V. A. Shchukin, V. P. Kalosha, J-R. Kropp, M. Agustin, G. Stępniak, J. P. Turkiewicz, and J-W. Shi. "Anti–waveguiding vertical–cavity surface–emitting laser at 850 nm: From concept to advances in high–speed data transmission." Optics express 26, no. 1 (2018): 445-453.
[4] Hamad, Wissam, Marwan Bou Sanayeh, Tobias Siepelmeyer, Hassan Hamad, and Werner HE Hofmann. "Small-signal analysis of high-performance VCSELs." IEEE Photonics Journal 11, no. 2 (2019): 1-12.
[5] Lang, Roy. "Injection locking properties of a semiconductor laser." IEEE Journal of Quantum Electronics 18, no. 6 (1982): 976-983.
[6] Feiste, Uwe. "Optimization of modulation bandwidth in DBR lasers with detuned Bragg reflectors." IEEE journal of quantum electronics 34, no. 12 (1998): 2371-2379.
[7] Chen, Da, Ye Liu, and Yonglin Yu. "Understanding the photon-photon resonance of DBR lasers using mode expansion method." Optical and Quantum Electronics 55, no. 1 (2023): 29.
[8] Matsuo, Shinji, Nikolaos-Panteleimon Diamantopoulos, Suguru Yamaoka, and Hidetaka Nishi. "Direct modulation of membrane distributed reflector lasers using optical feedback." In 2021 Optical Fiber Communications Conference and Exhibition (OFC), pp. 1-4. IEEE, 2021.
[9] Lau, Erwin K., Liang Jie Wong, and Ming C. Wu. "Enhanced modulation characteristics of optical injection-locked lasers: A tutorial." IEEE Journal of Selected Topics in Quantum Electronics 15, no. 3 (2009): 618-633.
[10] Lau, Erwin K., Xiaoxue Zhao, Hyuk-Kee Sung, Devang Parekh, Connie Chang-Hasnain, and Ming C. Wu. "Strong optical injection-locked semiconductor lasers demonstrating> 100-GHz resonance frequencies and 80-GHz intrinsic bandwidths." Optics Express 16, no. 9 (2008): 6609-6618.
[11] Dalir, Hamed, and Fumio Koyama. "Bandwidth enhancement of single-mode VCSEL with lateral optical feedback of slow light." IEICE Electronics Express 8, no. 13 (2011): 1075-1081.
[12] Heidari, Elham, Hamed Dalir, Moustafa Ahmed, Volker J. Sorger, and Ray T. Chen. "Hexagonal transverse-coupled-cavity VCSEL redefining the high-speed lasers." Nanophotonics 9, no. 16 (2020): 4743-4748.
[13] Heidari, Elham, Moustafa Ahmed, Hamed Dalir, Ahmed Bakry, Ahmed Alshahrie, and Volker J. Sorger. "VCSEL with multi-transverse cavities with bandwidth beyond 100 GHz." Nanophotonics 10, no. 14 (2021): 3779-3788.
[14] San Miguel, M., Q. Feng, and Jerome V. Moloney. "Light-polarization dynamics in surface-emitting semiconductor lasers." Physical Review A 52, no. 2 (1995): 1728.
[15] Martın-Regalado, J., M. San Miguel, N. B. Abraham, and F. Prati. "Polarization switching in quantum-well vertical-cavity surface-emitting lasers." Opt. Lett 21, no. 5 (1996): 351-353.
[16] Martin-Regalado, Josep, F. Prati, Maxi San Miguel, and N. B. Abraham. "Polarization properties of vertical-cavity surface-emitting lasers." IEEE Journal of Quantum Electronics 33, no. 5 (1997): 765-783.
[17] Homayounfar, Ali, and Michael J. Adams. "Locking bandwidth and birefringence effects for polarized optical injection in vertical-cavity surface-emitting lasers." Optics communications 269, no. 1 (2007): 119-127.
[18] Al-Seyab, Rihab, Kevin Schires, Antonio Hurtado, Ian D. Henning, and Michael J. Adams. "Dynamics of VCSELs subject to optical injection of arbitrary polarization." IEEE Journal of Selected Topics in Quantum Electronics 19, no. 4 (2013): 1700512-1700512.
[19] Pusch, Tobias, Markus Lindemann, Nils C. Gerhardt, Martin R. Hofmann, and Rainer Michalzik. "Vertical-cavity surface-emitting lasers with birefringence splitting above 250 GHz." Electronics Letters 51, no. 20 (2015): 1600-1602.

[20] Hurtado, Antonio, Ana Quirce, Angel Valle, Luis Pesquera, and Michael J. Adams. "Nonlinear dynamics induced by parallel and orthogonal optical injection in 1550 nm vertical-cavity surface-emitting lasers (VCSELs)." Optics express 18, no. 9 (2010): 9423-9428.
[21] Lindemann, Markus, Gaofeng Xu, Tobias Pusch, Rainer Michalzik, Martin R. Hofmann, Igor Žutić, and Nils C. Gerhardt. "Ultrafast spin-lasers." Nature 568, no. 7751 (2019): 212-215.
[22] Bava, G. P., P. Debernardi, and L. Fratta. "Three-dimensional model for vectorial fields in vertical-cavity surface-emitting lasers." Physical Review A 63, no. 2 (2001): 023816.
[23] Debernardi, Pierluigi, and Gian Paolo Bava. "Coupled mode theory: a powerful tool for analyzing complex VCSELs and designing advanced device features." IEEE Journal of selected topics in quantum electronics 9, no. 3 (2003): 905-917.
[24] Prati, F., A. Tesei, L. A. Lugiato, and R. J. Horowicz. "Stable states in surface-emitting semiconductor lasers." Chaos, Solitons & Fractals 4, no. 8-9 (1994): 1637-1654.
[25] D'Alessandro M., et al., "Transverse Coupled Cavity VCSELs: Bridging Ultrabroadband Dynamics To Optical Supermodes", IEEE Photonics Journal, Conference on Numerical Simulation of Optoelectronic Devices (NUSOD-2023), 2024 (submitted)